# Continuous Test of Ilmenite-Based Oxygen Carriers for Chemical Looping Combustion in a Dual Fluidized Bed Reactor System

**ARTICLE** *in* INDUSTRIAL & ENGINEERING CHEMISTRY RESEARCH · OCTOBER 2013

Impact Factor: 2.59 · DOI: 10.1021/ie4025209



**4 AUTHORS**, INCLUDING:

Hongming Sun
Tsinghua University
**5** PUBLICATIONS **48** CITATIONS
SEE PROFILE

Ningsheng Cai
Tsinghua University
**138** PUBLICATIONS **1,797** CITATIONS
SEE PROFILE

I&EC research
Industrial & Engineering Chemistry Research

Article

pubs.acs.org/IECR

# Continuous Test of Ilmenite-Based Oxygen Carriers for Chemical Looping Combustion in a Dual Fluidized Bed Reactor System

Jinhua Bao, Zhenshan Li,* Hongming Sun, and Ningsheng Cai

Key Laboratory for Thermal Science and Power Engineering of Ministry of Education, Beijing Municipal Key Laboratory for $CO_2$ Utilization & Reduction, Department of Thermal Engineering, Tsinghua University, Beijing 100084, China

**ABSTRACT:** Raw ilmenite was tested as an oxygen carrier for chemical looping combustion (CLC) in a dual fluidized bed reactor for 100 h. After this 100 h test, 21 wt % of the total used raw ilmenite was impregnated with 10 wt % potassium (K). The K-impregnated ilmenite mixed with the remaining used raw ilmenite was tested in the same reactor for 40 h. During the 100 h test, raw ilmenite showed a low reduction reactivity, which only converted 60% CO into $CO_2$ at 900 °C with a 4.2 kPa pressure drop in the fuel reactor. By impregnating merely 21% of the used raw ilmenite with 10% $K^+$, the reactivity was promoted and thus the CO conversion was improved to over 78.5% under the same conditions. Although reactivity deterioration of the 10% $K^+$ promoted ilmenite related to $K^+$ volatilization was found, the CO conversion only dropped from 100% to 89% even after 28 h of continuous operation. The effect of different operation parameters on gas conversion behavior was investigated with raw ilmenite; the gas flow rate and temperature of the fuel reactor turned out to be the critical parameters. However, the reduction reactivity of the 10% $K^+$ promoted ilmenite was not affected by temperature as much as that of the raw ilmenite, and therefore, it can be used in a wide temperature range (900−600 °C). During use of both the raw and promoted ilmenites, no sintering or agglomeration occurred; the proportions of mass loss caused by fragmentation and attrition to the total solid inventory were low, only 0.87% (100 h) and 0.71% (40 h). Both ilmenite carriers showed good mechanical strength and stability. The 10% $K^+$ promoted ilmenite was proven to be one promising oxygen carrier for chemical looping combustion.

## 1. INTRODUCTION

Chemical looping combustion (CLC) is one of the most promising technologies to separate $CO_2$ without energy penalty.[1,2] CLC is based on the transfer of oxygen from air to the fuel by means of a so-called "oxygen carrier" that circulates between the fuel reactor and the air reactor. In the fuel reactor, the oxygen carrier is reduced by oxidizing the fuel to $CO_2$ and $H_2O$. The reduced oxygen carrier is then transferred to the air reactor and oxidized by air before starting a new cycle. Theoretically, a pure steam of $CO_2$ can be obtained directly after condensing the $H_2O$ from the exhaust of the fuel reactor. Therefore, CLC has the advantage of separating $CO_2$ intrinsically during the unmixed combustion process without an additional step and loss of efficiency. To put it another way, the CLC concept requires a high-purity of $CO_2$ ready for sequestration after $H_2O$ condensation. However, in practice, the purity of $CO_2$ mainly depends on the conversion of the fuel gases, such as natural gas or syngas (CO and $H_2$) from solid char gasification. A high fuel gas conversion is thus desired for the purpose of obtaining a high concentration of $CO_2$. The conversion of fuel gas is related to its reaction with solid oxygen carriers within the gas residence time in the fuel reactor. In this gas−solid reaction, the reduction reactivity of oxygen carriers by fuel gases determines the conversion of fuel gases. A high fuel gas conversion requires a high reduction reactivity of the oxygen carrier.

For CLC with gaseous fuels, synthetic oxygen carriers based on the oxides of the metals Ni, Co, Fe, Cu, and Mn have been proven to have high reactivity for a nearly complete conversion of fuels.[3−6] However, these synthetic carriers are relatively expensive, and some of them, such as Ni- and Co-based, are toxic. Also, the preparation of the synthetic oxygen carriers is costly and sometimes is not environmentally friendly. These characteristics make the synthetic carriers not practical for CLC directly using solid fuels, such as coal and biomass. This is mainly because the existence of solid ash derived from solid fuels puts new restraints on oxygen carriers. The solid ash could not only affect the lifetime of the oxygen carrier but also cause a partial loss of the oxygen carrier during ash removal. Therefore, the direct application of CLC to solid fuels requires low-cost and easily available oxygen carriers, such as natural minerals, rather than the synthetic carriers. Ilmenite, a natural mineral composed of $FeTiO_3$, is a low cost, attractive material and has been tested extensively.[7−14] Although ilmenite has the advantages of low cost and availability, it shows a low reduction reactivity. This means that a large bed inventory is required for a complete conversion of syngas in the fuel reactor, which will increase the reactor scale along with the capital cost.

Previous works have found that the reactivity of ilmenite can be promoted by introducing foreign ions ($K^+$, $Na^+$, and $Ca^{2+}$).[15,16] The reduction reactivity and stability over redox cycles of different foreign ion promoted ilmenites have been investigated in both a thermogravimetric analyzer (TGA) and a laboratory-scale fluidized bed reactor. Potassium (K) was reported to be the best option for reactivity enhancement. Ilmenite promoted by 10 wt % or 15 wt % $K^+$ obtained a reactivity 6.5 or 7 times faster than that of the activated raw ilmenite, respectively.[16] Neither agglomeration nor obvious

**Received:** August 1, 2013
**Revised:** September 24, 2013
**Accepted:** September 26, 2013
**Published:** September 26, 2013





dx.doi.org/10.1021/ie4025209 | *Ind. Eng. Chem. Res.* 2013, 52, 14817−14827

fragmentation and attrition were found during as long as 100 successive cycles in the batch fluidized bed.[15] However, the performance of the promoted ilmenite has not been evaluated yet during long-term operation in an interconnected fluidized bed reactor, which is the most likely practical industrial-scale facility for CLC technology.[17] This evaluation is utterly crucial to obtain more knowledge about the behavior of the promoted ilmenite in the practical reactor during extended operation periods.

Accordingly, the objectives of the present research were to investigate the potassium promoted ilmenite in a dual-fluidized bed reactor by comparing to the raw ilmenite from the aspects of the reduction reactivity or gas conversion, long-term chemical and mechanical stability, and effect of operation conditions.

## 2. EXPERIMENTAL SECTION

**2.1. Ilmenite Oxygen Carriers.** Two types of oxygen carriers—the raw ilmenite and the 10 wt % $K^+$ promoted ilmenite—were tested in this study. The raw ilmenite was preoxidized to its most oxidized state by thermally treating the fresh ilmenite at 950 °C in air for 24 h.[18] The raw ilmenite particle has a density of 4246 kg/m$^3$ and a surface area of 0.64 m$^2$/g. Raw ilmenite that experienced 100 h of continuous operation in a dual fluidized bed reactor was used to prepare the 10 wt % $K^+$ promoted ilmenite through a wet impregnation method. $K_2CO_3$ was employed as the precursor. The mass ratio of the alkali metal ion $K^+$ to ilmenite was controlled at 10 wt %. For simplicity, here we designate the 10 wt % $K^+$ promoted ilmenite as K10-ilmenite. Before experiments, K10-ilmenite was calcined in a muffle oven at 900 °C for 30 min, in order to partially decompose the containing $K_2CO_3$. Both ilmenite particles used were 125−300 $\mu$m in size. More details on the preparation, physical properties, and chemical composition of these materials can be found in two previous publications.[15,16]

**2.2. Dual Fluidized Bed Reactor System.** The experiments were conducted in a continuous operation system consisting of two interconnected fluidized beds. Figure 1 shows a general view over the whole reactor system. The setup is basically composed of a fuel reactor (FR), where oxygen carriers are reduced by reducing agent; an air reactor (AR), where the particles circulating back from the FR through a lower loop seal (LS) are reoxidized; a riser, which transports solids from AR to FR via a cyclone (a gas−solid separator); and an upper loop seal. The fuel reactor consists of a bubbling fluidized bed with an inner diameter of 50 mm and a bed height of 1000 mm. The air reactor consists of a bubbling fluidized bed with an inner diameter of 50 mm and a bed height of 100 mm, followed by a riser with an inner diameter of 20 mm and a height of 3300 mm. Introduction of secondary air at the top of the bubbling bed assists with particle entrainment. The upper and lower U-shaped loop seals are designed for eliminating gas leakages between AR and FR. Both loop seals are 60 mm long, 40 mm wide, and 300 mm high. The oxygen carrier particles can be fed into the system through a double valve feeder on top of the fuel reactor. The gas leakage was tested in an equivalent cold model reactor and was further verified in this hot model reactor at both ambient and high temperatures under different operating conditions.

The system is not autothermal due to a small scale. The two reactors are heated up to the desirable operating temperatures with different electrical furnaces. Other parts, including the riser, the cyclone, and the loop seals, are heated up by

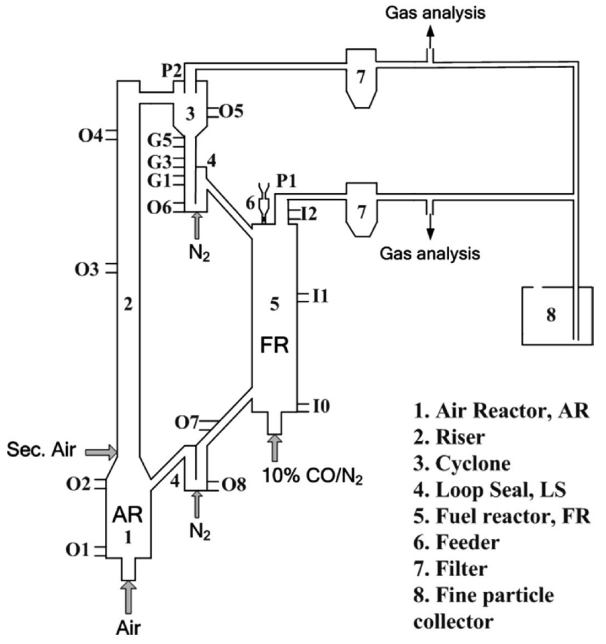


**Figure 1.** Configuration of the dual fluidized bed reactor system for CLC.

resistance wires with insulation. Temperatures in different locations of the entire system are monitored by K-type thermocouples. In order to better monitor the operation state of the unit, there are 16 pressure taps (O1−O8, I0−I2, G1, G3, G5, P1, and P2) distributed in important locations, as illustrated in Figure 1. O1−O8 and I0−I2 are used to monitor the solid circulation of the entire loop; G1, G3, and G5 are adopted to monitor the solid's height in the left chamber of the upper loop seal and the returning leg, as well as evaluate the real-time solid circulation rate; P1 and P2 are measured to monitor the downstream blockage. A data acquisition system is used to record the pressure signals from pressure transducers connected to the pressure taps. The exhausted gas from each reactor first passes through a filter separately to remove the particles carried by the gas and then goes to one fine particle collector together before finally discharging into the environment. After exiting from the filter, the gas from each reactor is continuously sampled and analyzed.

The real-time solid circulation rate $G_s$ was measured based on the pressure signals of G1, G3, and G5. Figure 2 shows the flow-sheet of the methodology used to measure $G_s$. During a stable operation, the gas flow rate of the upper loop seal (<1.8 $L_N$/min STP) was gradually increased to ensure that the solid's height was lower than G1 ($\Delta p$(G1 − G3) = 0). Then, the inlet gas of the upper LS was shut off to let the solid particles accumulate. The start time was when the pressure between G1 and G3 started to increase, and the end time was when the pressure between G3 and G5 started to increase. In this way, the duration $\Delta t$ (s) for the particles to accumulate from G1 to G3 was known. The above steps were repeated twice; finally the average accumulation time $\overline{\Delta t}$ (s) could be calculated. With the known bulk density of the ilmenite $\rho$ (2319 kg/m$^3$), the volume between G1 and G3 $V$ ($8.4 \times 10^{-5}$ m$^3$), the cross-sectional area of the riser $A$ ($3.14 \times 10^{-4}$ m$^2$), and the measured average accumulation time $\overline{\Delta t}$ (s), the solid circulation rate $G_s$ (kg/m$^2$·s) can be calculated according to eq 1.


dx.doi.org/10.1021/ie4025209 | Ind. Eng. Chem. Res. 2013, 52, 14817−14827

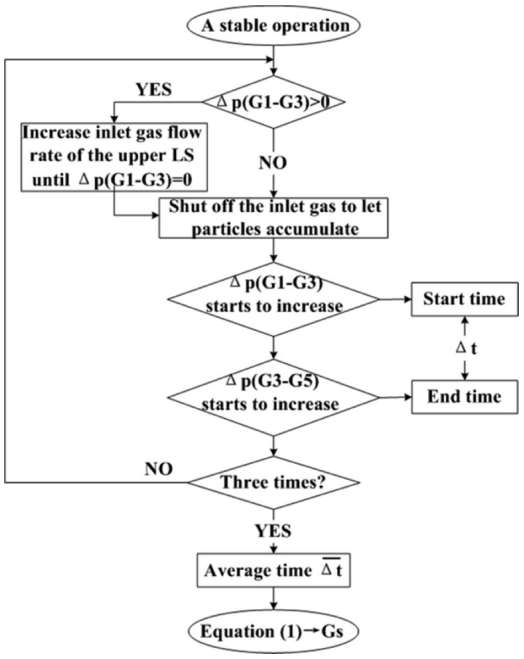


**Figure 2.** Flow-sheet of the methodology used to measure the real-time solid circulation rate $G_s$.

$$G_s = \frac{\rho V}{A\overline{\Delta t}} \tag{1}$$

After accomplishing the measurement of $G_s$, the operation was set back to the original state.

**2.3. Operation Conditions.** Two continuous extended operations (100 h for the raw ilmenite and 40 h for 10% $K^+$ promoted ilmenite (K10-ilmenite) mixed with the used raw ilmenite) were performed. Both operations were continuous without interruption, even at night. The total solid inventory of the system was 7302 g for the raw ilmenite and 7000 g for K10-ilmenite mixed with raw ilmenite. After 100 h operation of the raw ilmenite, ~21% of the total used raw ilmenite, that is, ~1500 g, was impregnated with 10 wt % $K^+$. The promoted ilmenite was mixed with the remaining used raw ilmenite and fed into the system for 40 h operation.

Before starting each operation, the system was fluidized with air and gradually heated to the desired temperature with solid circulation. During the heating up process, the flow rates in different parts were adjusted simultaneously. After reaching the preset temperature, the temperatures of both reactors were kept constant at approximately 900 °C, except when considering the effect of the fuel reactor temperature; the temperatures of the riser, the cyclone, and the loop seals were about 700 °C, which were limited by the power of the resistance wires. The fluidizing gas of the fuel reactor and the two loop seals was switched from air to $N_2$. After the fuel reactor was purged by $N_2$, the reducing gas ~10 vol % CO/$N_2$ was switched on and the continuous operation started. Table 1 gives the gas flow rates at different locations during both operations. The gas flows introduced in the air reactor were 5 $L_N$/min as primary air and 33 $L_N$/min as secondary air, corresponding to a total gas velocity in the riser of 2.0 m/s. The flow rate of the reducing gas (~10 vol % CO/$N_2$) for the fuel reactor was 4 $L_N$/min. The gas velocities at 900 °C in FR and the bottom bubbling fluidized bed of AR were 3.3 and 4.2 times the minimum fluidization velocity (0.04 m/s at 900 °C) of the ilmenite particle, respectively. The upper and lower loop seals were fluidized with 1 $L_N$/min and 2 $L_N$/min of $N_2$, respectively. During the 100 h operation of the raw ilmenite, the effects of different operation conditions, including the FR temperature, the reducing gas flow rate, and the solid circulation rate, were considered. Since there was no gas leakage, during each operation, the $CO_2$ and CO concentrations from the exit stream of FR and the $O_2$ concentration from the exhausted gas of AR were continuously analyzed. However, the detected gas concentrations of $CO_2$ and CO from FR were diluted by $N_2$ from the upper loop seal; likewise, the detected gas concentration of $O_2$ was diluted by $N_2$ from the lower loop seal. Therefore, during the data processing, the real gas concentrations were obtained after eliminating the dilution effect of $N_2$ flows of loop seals.

**Table 1. Gas Flow Rates ($L_N$/min, STP) at Different Locations during Both 100 and 40 h Operations, Except When Considering the Effect of the FR Gas Flow Rate and the Solid Circulation Rate**

| location | fluidizing gas | gas flow rate ($L_N$/min) |
|---|---|---|
| AR | primary air | 5 |
| | secondary air | 33 |
| FR | ~10 vol % CO | 4 |
| lower LS | $N_2$ | 2 |
| upper LS | $N_2$ | 1 |

**2.4. Data Evaluation.** One key index for CLC is the conversion of fuel gas (CO in this study). It determines the $CO_2$ purity and the sequestration of the captured $CO_2$, as has been emphasized in the Introduction. Based on the outlet $CO_2$ and CO concentrations ($C_{CO_2}$ and $C_{CO}$) of the fuel reactor, the conversion of CO, $x_{CO}$, can be calculated according to eq 2.

$$x_{CO} = \frac{C_{CO_2}}{C_{CO} + C_{CO_2}} \tag{2}$$

The mass loss ($\Delta m$) of oxygen carrier particles caused by fragmentation and attrition, which determines the final cost of the oxygen carrier, is another key index for CLC. The fragmentation and attrition ratio $\delta_m$ (%) is the proportion of this mass loss $\Delta m$ (g) to the total ilmenite inventory $m$ (g) added in the system, as defined by eq 3.

$$\delta_m = \frac{\Delta m}{m} \times 100 \tag{3}$$

## 3. RESULTS AND DISCUSSION

**3.1. 100 h Continuous Operation of the Raw Ilmenite.** Raw ilmenite was continuously tested as an oxygen carrier for CLC in the dual-fluidized bed reactor for 100 h, which will provide a comparison for the following test on the promoted ilmenite. No sintering or agglomeration of the ilmenite particles was found during this long-term operation, which shows one advantage of the natural ilmenite. Also, the reactor system was continuously running for as long as 100 h without any problems; this demonstrated the feasibility and robustness of the facility. Figure 3 shows the off-gas concentrations and the pressure drop of the fuel reactor during the 100 h operation. Based on the variation of the gas concentrations and pressure signals, the operation can be divided into six stages. Except in stage 5, where various conditions were chosen, the system was operated under a uniform condition: both the air and fuel reactors were at 900 °C, and the gas flow rates were kept


dx.doi.org/10.1021/ie4025209 | Ind. Eng. Chem. Res. 2013, 52, 14817−14827

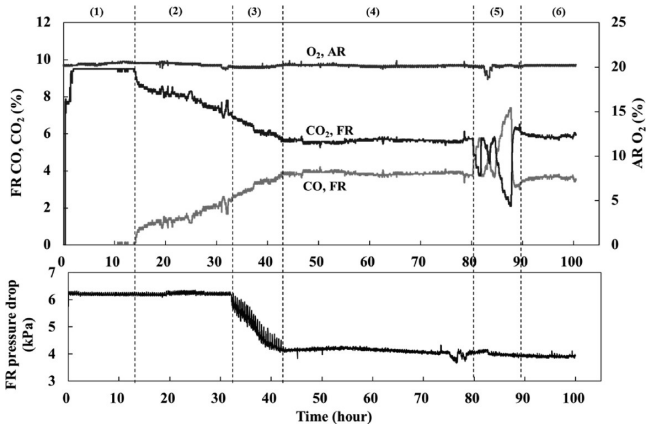


**Figure 3.** Flue gas concentrations (CO and $CO_2$ from FR; $O_2$ from AR) and pressure drop of the fuel reactor as a function of time during 100 h of continuous operation of the raw ilmenite. Except in stage 5, where various conditions were chosen, the system was operated under a uniform condition with both AR and FR being at 900 °C, and the gas flow rates were listed in Table 1.

constant as listed in Table 1. In stage 1 of Figure 3, during the first 13.7 h, there was a complete conversion of CO. However, in stage 2, unconverted CO started to appear in the flue gas. This unconverted CO concentration increased gradually with a decrease of $CO_2$ concentration simultaneously. Correspondingly, the CO conversion decreased from 100% to 73% during 19.4 h. At this time, the solid inventory in the fuel reactor still remained the same as in stage 1, as indicated by the pressure drop of the fuel reactor. Therefore, the decrease of CO conversion was most likely caused by a reduction reactivity deterioration of the raw ilmenite. The reactivity activation of ilmenite, as reported in the published works,[7−9,15] should be accomplished earlier in stage 1, which was not reflected in the variation of the flue gas concentrations. In stage 3, the unconverted CO continued to increase, indicating a further decrease of CO conversion. The conversion of CO was reduced to 60% at the end of this stage (43.2 h). In this stage, the pressure drop of the fuel reactor gradually decreased from 6.2 to 4.2 kPa within 10 h. This suggested that there was a gradual decrease of the fuel reactor inventory. From this aspect, the continuous decrease of CO conversion could be caused by a reduced fuel reactor inventory. The reactivity decline of ilmenite may still exist in this stage, which diminished the CO conversion simultaneously. In stage 4, both the CO and $CO_2$ concentrations along with the FR pressure drop became stable. The CO conversion was stabilized at approximately 60%. A stable reactivity of the raw ilmenite was obtained and maintained. In stage 5 during the stable operation, various conditions of the FR gas flow rate, the FR temperature, and the solid circulation rate were chosen to study their effect on the gas conversion behavior in the fuel reactor. In this way, the critical operation parameters for gas conversion can be known. The results of stage 5 were discussed later in sections 3.1.1−3.1.3. After operating under different conditions for 10 h, the original operating conditions were restored. Along with this, the stable flue gas distribution and CO conversion were reinstated, as shown in the final stage 6. This demonstrated that the raw ilmenite maintained its stable reactivity after operating under different conditions. The stable reduction reactivity was totally maintained for 56.7 h from the beginning of stage 4 until the end of stage 6. The detected $O_2$ concentration from the air reactor was kept constant at ∼20% during the entire 100 h, except for a small fluctuation in stage 5. It should be mentioned that the pressure drop of the fuel reactor actually showed a gradually decreasing trend from 51.7 to 100 h; the decrease was 70 Pa in stage 4 and totally 167 Pa in stages 5 and 6. However, this slow decrease is negligible, so the fuel reactor pressure drop can be regarded as being stable.

The drop of the fuel reactor pressure within 10 h in stage 3 was due to a low efficient cyclone, which caused the particle elutriation to the filter. As a result, the inventory remaining in the reactor was reduced. This occurrence finally decreased the conversion of CO. The raw ilmenite inventory in the system was 7302 g initially, which decreased to only 5459 g after 100 h, with 1838 g being elutriated to the filter. The particle elutriation mostly occurred during stage 3 according to the fuel reactor pressure drop. More detailed analysis on the elutriated particles was given in section 3.3.

*3.1.1. Effect of the FR Gas Flow Rate.* The effect of the reducing gas flow rate on gas conversion was first considered during stage 5 in Figure 3. Different flow rates of 10 vol % CO/$N_2$ (4, 5, 6, 7 $L_N$/min, STP) were chosen. Other parameters were kept constant. Figure 4 shows the variation of flue gas

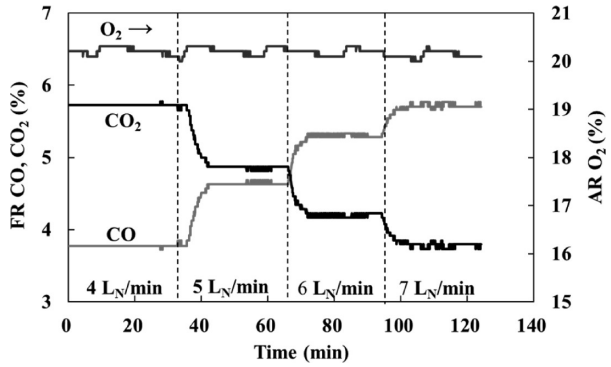


**Figure 4.** Flue gas concentrations (CO and $CO_2$ from FR; $O_2$ from AR) with time at different reducing gas flow rates of the fuel reactor (stage 5 of Figure 3). Other gas flow rates were kept the same as in Table 1. Both the air and fuel reactors were at 900 °C.

concentrations. As the inlet flow rate of the reducing gas increased, the gas residence time in the fuel reactor was shortened. Because of this, the unconverted CO at the exit stream of the fuel reactor increased while the oxidation product $CO_2$ decreased. The conversion of CO was thus reduced. The CO conversion was 60% with a FR gas flow rate of 4 $L_N$/min, which decreased to only 40% when this flow rate increased to 7 $L_N$/min. However, the increase of the FR gas flow rate did not cause any variation of the $O_2$ concentration from AR.

*3.1.2. Effect of the FR Temperature.* A subsequent study of the effect of the fuel reactor temperature on gas conversion was carried out during stage 5 of Figure 3. Figure 5 shows the CO and $CO_2$ concentrations of the flue gas from the fuel reactor at different fuel reactor temperatures from 900 to 650 °C. At each temperature, the system was steadily operated for 30 min. It can be seen from Figure 5 that as the fuel reactor temperature lowered, there was an obvious increase of CO concentration with a decrease of $CO_2$ concentration at the outlet of fuel reactor, which corresponded to a reduced CO conversion. The conversion of CO decreased from 60% at 900 °C to 22% at 650 °C. This was because the reduction reactivity of the raw ilmenite decreased at lower temperatures. Moreover, the


dx.doi.org/10.1021/ie4025209 | Ind. Eng. Chem. Res. 2013, 52, 14817−14827

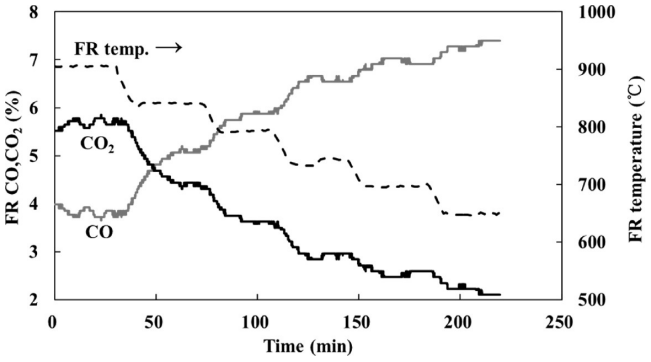


**Figure 5.** Concentrations of CO and $CO_2$ from the flue gas of the fuel reactor with time at different fuel reactor temperatures (stage 5 of Figure 3). Gas flow rates were listed in Table 1.

increase of unconverted CO concentration was less at low temperatures than at high temperatures. In other words, the decrease of CO conversion was less at low temperatures than at high temperatures. For example, when the FR temperature decreased from 700 to 650 °C, the decrease of CO conversion was only 5% (from 27% to 22%), which is much less than the 14% decrease (from 60% to 46%) from 900 to 850 °C. This result demonstrated that the decrease of ilmenite's reduction rate was slower at low temperatures than at high temperatures. During this entire period, the $O_2$ concentration from AR was not affected either.

*3.1.3. Effect of the Solid Circulation Rate.* A final consideration during stage 5 of Figure 3 was the effect of solid circulation rate on gas conversion behavior. Different solid circulation rates were obtained by changing the flow rate of the secondary air in the air reactor. A stable operation under each different status was maintained for 30 min. Figure 6 represents

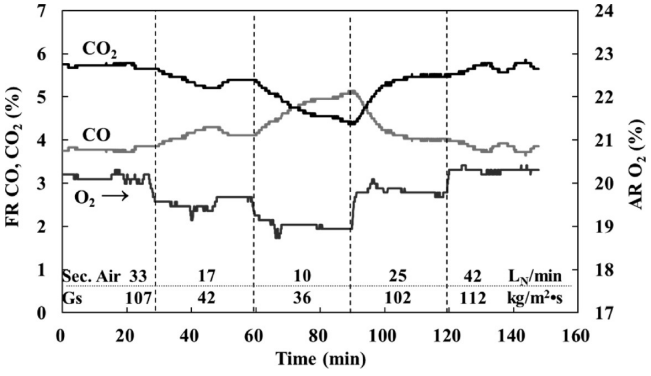


**Figure 6.** Flue gas concentrations (CO and $CO_2$ from FR; $O_2$ from AR) with time at different solid circulation rates by changing the secondary air flow rate of the air reactor (stage 5 of Figure 3). Other gas flow rates were kept the same as in Table 1. Both the air and fuel reactors were at 900 °C.

the flue gas concentrations in both air and fuel reactors during this period. The flow rate of the secondary air decreased from 33 $L_N$/min to 10 $L_N$/min and then increased to 42 $L_N$/min with the solid circulation rate $G_s$ decreasing from 107 kg/m$^2$·s to 36 kg/m$^2$·s and increasing to 112 kg/m$^2$·s afterward, as illustrated by Figure 6. As the solid circulation rate decreased, the oxidized ilmenite entering into the fuel reactor was reduced, corresponding to less oxygen available for oxidizing the reducing gas CO. As a result, the conversion of CO decreased. This is the reason why the CO concentration increased and $CO_2$ concentration decreased at a smaller solid circulation rate, and vice versa. However, the effect of solid circulation rate on gas conversion was not as obvious as the effect of FR gas flow rate and FR temperature. When $G_s$ decreased from 107 kg/m$^2$·s to 36 kg/m$^2$·s, the CO conversion only decreased from 60% to 48%. Besides the effect on the gas conversion, the decrease of solid circulation rate also caused a decrease of $O_2$ concentration in the air reactor off-gas, and vice versa. The $O_2$ concentration decreased from 20.1% to 18.94% when $G_s$ decreased from 107 kg/m$^2$·s to 36 kg/m$^2$·s. This is mainly because the total inlet oxygen amount was reduced when the flow rate of the secondary air was lowered to obtain a smaller solid circulation rate.

Comparing the studied three parameters above, both the FR flow rate and the FR temperature have strong effects on the gas conversion, whereas the effect of the solid circulation rate is relatively small. Therefore, in the CLC process, in order to gain a high conversion of syngas to increase the $CO_2$ purity, the parameters of the fuel reactor, including the temperature as well as the gas flow rate, should be well controlled. At a given reducing gas flow rate, the maintenance of a high fuel reactor temperature is required when using the raw ilmenite as an oxygen carrier. Meanwhile, among the three parameters discussed above, only the effect of fuel reactor temperature on gas conversion is directly determined by the oxygen carrier's reduction reactivity. The effects of the FR gas flow rate and the solid circulation rate were related to the hydrodynamics. From this aspect, the effects of the fuel reactor temperature on gas conversion, which directly depend on the carrier's reactivity, deserve more attention when comparing two oxygen carriers. Therefore, in the following study of the 10% $K^+$ promoted ilmenite, only the effect of fuel reactor temperature was considered.

**3.2. 40 h Continuous Operation of the 10% $K^+$ Promoted Ilmenite.** After 100 h of continuous operation of the raw ilmenite, ~21% (~1500 g) of the total used raw ilmenite in the size of 125−300 $\mu$m (the fine particles <125 $\mu$m were removed) was impregnated with 10 wt % $K^+$. The final product of the 10% $K^+$ promoted ilmenite (K10-ilmenite) was 1585 g (125−300 $\mu$m). K10-ilmenite mixed with the remaining raw ilmenite from 100 h of operation was continuously tested for about 40 h in the dual fluidized bed reactor under the same conditions as those for the 100 h operation. Figure 7 shows the flue gas concentrations of both air and fuel reactors and the fuel reactor pressure drop during the 40 h operation. Although there was existence of potassium K and the release of K during combustion could cause sintering of particles, bed agglomeration, or even downstream corrosion, none of these problems occurred during the 40 h. The particles discharged from the system at the end did not show any trace of sintering or agglomeration. The entire 40 h operation included six stages, as shown in Figure 7.

In stage 1, the bed material was merely 600 g of K10-ilmenite well mixed with 5415 g of raw ilmenite, totally 6015 g. Here, the thermal decomposition of $K_2CO_3$, which was contained in the 600 g of K10-ilmenite, was accomplished prior to stage 1. The pressure drop of the fuel reactor was approximately 4.5 kPa, which was similar to the pressure drop of 4.2 kPa in stage 4 of Figure 3 for pure raw ilmenite. This meant that, in both cases, the fuel reactor inventories were in the same level. The fuel reactor temperature increased from 700 to 800 °C, and finally to 900 °C, in order to evaluate the effect of temperature


dx.doi.org/10.1021/ie4025209 | Ind. Eng. Chem. Res. 2013, 52, 14817−14827

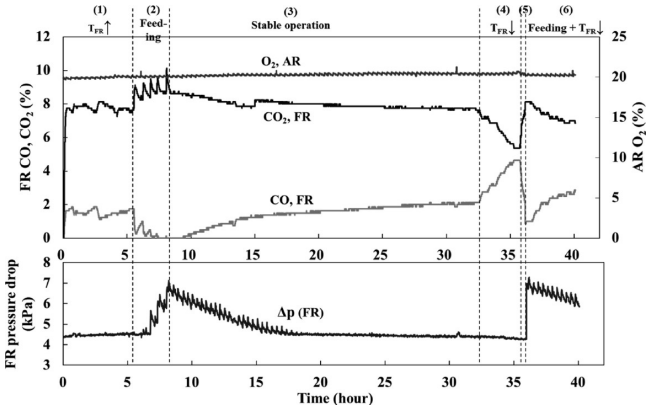


**Figure 7.** Flue gas concentrations (CO and $CO_2$ from FR; $O_2$ from AR) and pressure drop of the fuel reactor as a function of time during 40 h continuous operation of K10-ilmenite mixed with the used raw ilmenite. Stage 1: 5415 raw ilmenite +600 g of K10-ilmenite; increase FR temperature from 700 to 900 °C. Stage 2: feed 985 g of K10-ilmenite separately in five batches. Stage 3: stable operation at 900 °C. Stage 4: decrease FR temperature from 900 to 650 °C. Stage 5: increase FR temperature back to 900 °C ; feed the elutriated particles (1280 g) at the end. Stage 6: decrease FR temperature from 900 to 600 °C. Gas flow rates were listed in Table 1.

on gas conversion with merely 600 g of K10-ilmenite contained in the reactor. A magnification of the concentration profiles for CO and $CO_2$ at different fuel reactor temperatures of stage 1 can be seen in Figure 8. Although the unconverted CO at the

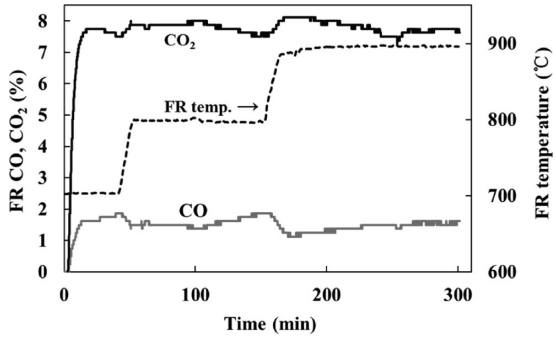


**Figure 8.** CO and $CO_2$ concentrations of the flue gas of the fuel reactor during increasing the fuel reactor temperature from 700 to 900 °C (stage 1 of Figure 7). Bed material: 5415 g of raw ilmenite + 600 g of K10-ilmenite.

outlet of the fuel reactor indeed decreased slightly at higher temperatures, it did not vary much within 700−900 °C and was in the range of 1.25−1.88%. This corresponded to a small variation of the CO conversion, which only varied between 87 and 80%. The conversion of CO with the presence of 600 g of K10-ilmenite, even at lower temperatures, was much higher than in the case of the pure raw ilmenite in stage 4 of Figure 3, where the unconverted CO was up to 3.93% and CO conversion was as low as 60% at 900 °C. The existence of K10-ilmenite did succeed in improving the gas conversion due to its promoted reduction reactivity by $K^+$. Meanwhile, the reactivity of K10-ilmenite tended to increase slightly as the temperature rose. However, the small variation at different temperatures indicated that the reduction temperature did not affect the promoted reactivity of K10-ilmenite much, at least during the initial reaction stage (∼5 h) of K10-ilmenite. In addition, it should be pointed out that, in Figure 8, the outlet CO concentration showed a slow increase at each temperature. This occurrence should be attributed to the reactivity deterioration of K10-ilmenite. This is also the reason why we did the continuous, long-term test on this promoted ilmenite to study its stability.

In stage 2, all the remaining K10-ilmenite (985 g) was fed directly into the fuel reactor separately in five batches; the added K10-ilmenite was 200 g in each of the first four batches and was 185 g in the final fifth batch. The duration of each batch was ∼30 min. The total solid inventory was 7000 g after feeding. During the feeding process, the pressure drop of the fuel reactor increased, which finally rose to about 7 kPa. The thermal decomposition of $K_2CO_3$ from the fresh K10-ilmenite immediately after feeding caused an abrupt increase of $CO_2$. The addition of more K10-ilmenite was aimed at achieving a complete conversion of CO. As seen from stage 2 of Figure 7, the outlet CO concentration decreased after each of the first three batches; it already decreased to 0.125% after the third batch, a nearly complete CO conversion. A complete conversion of CO was obtained after the feeding of the fourth and fifth batches. After the fifth batch, there were totally 1585 g of K10-ilmenite contained in the reactor.

In stage 3, all the 1585 g of K10-ilmenite along with the used raw ilmenite (5415 g) was tested for about 24 h under one uniform condition with the fuel reactor being at 900 °C and the gas flow rates being the same as in Table 1. At the beginning, the conversion of CO still remained complete and lasted until 9.2 h. However, afterward, there was unconverted CO appearing in the exhaust gas of the fuel reactor and this CO concentration gradually increased with a decrease of $CO_2$. The CO concentration reached to 1.38% at 15 h within ∼6 h. After 15 h, the increase of CO slowed down. The unconverted CO only rose to 2.13% at the end of stage 3 within 17.5 h. At the same time, there was a gradual decrease of the fuel reactor pressure from 8 h (the beginning of stage 3) to 17 h. The pressure dropped from 6.8 to 4.5 kPa within 9 h. This was caused by the particle elutriation from the cyclone to the filter. However, afterward, the fuel reactor pressure was stabilized at ∼4.5 kPa. The particle elutriation, which reduced the solid inventory in the system, was one possible explanation for the relatively fast increase of CO concentration in the early stage 3. At the later period of stage 3, there was still a slow increase of CO even when the fuel reactor pressure was stable. This suggested that the particle elutriation was not the only reason for the increase of the unconverted CO. Another possible reason for the CO increase was the reactivity deterioration of K10-ilmenite, as also mentioned during the discussion of stage 1. The reactivity deterioration of K10-ilmenite could be related to the volatility of the alkali metal K. Some K released into the gas phase through volatilization and was carried downstream by the gas, resulting in a loss of K. The partial pressure of K in the gas phase determined the volatilization rate of K. In the air reactor, due to the addition of secondary air, the total gas flow rate was much larger than the flow rates of other parts as well as the flow rate (2 $L_N$/min) used in the laboratory-scale fluidized bed previously.[15] As a result, the partial pressure of K in the gas phase of the air reactor was much less, corresponding to a faster volatilization of K. In other words, the loss of K in the dual fluidized bed reactor, especially in the air reactor, was much more intense than that in the laboratory-scaled reactor. The X-ray fluorescence (XRF) analysis revealed that the final particles in the reactor after 40 h operation contained 46.89% $TiO_2$,


dx.doi.org/10.1021/ie4025209 | Ind. Eng. Chem. Res. 2013, 52, 14817−14827

44.19% $Fe_2O_3$, and 2.91% $K_2O$, giving K/(Ti + Fe) = 4.09%, which was less than half of the ratio (8.58%) for K10-ilmenite after 40 redox cycles in the laboratory-scale fluidized bed.[16] Previous studies have reported that the existence of K can assist in the promotion of pore structures of the ilmenite particles and the formation of the alkali-rich phase, that is, $K_{1.46}Ti_{7.2}Fe_{0.8}O_{16}$, may behave as a catalyst for the reduction reaction.[15,16] Therefore, the loss of K will weaken these positive effects and then reduce the reactivity promotion effect of K. This is the most likely reason for the reactivity deterioration. Although there were reactivity deterioration and particle elutriation, the conversion of CO with the mixing of K10-ilmenite in stage 3 of Figure 7 was still over 78.5%, which was much higher than 60% for the pure raw ilmenite in stage 4 of Figure 3.

In stage 4, after K10-ilmenite had been tested for 32.5 h, the effect of fuel reactor temperature on gas conversion was investigated. During this stage, the fuel reactor pressure remained almost stable at 4.3 kPa. Figure 9a shows a magnification of the CO and $CO_2$ concentrations at different fuel reactor temperatures from 900 to 650 °C in stage 4 of Figure 7.

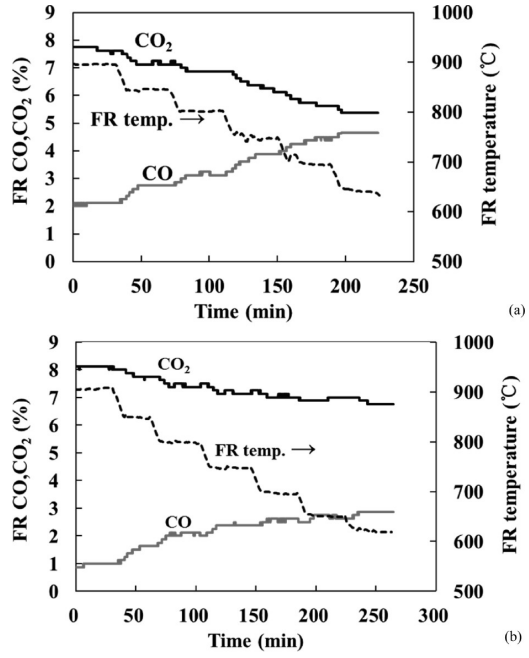


**Figure 9.** CO and $CO_2$ concentrations of the flue gas of the fuel reactor at different fuel reactor temperatures. (a) Stage 4 of Figure 7, $\Delta p$(FR) ≈ 4.3 kPa; (b) stage 6 of Figure 7, after feeding the elutriated particles (1280 g) from the filter into the fuel reactor $\Delta p$(FR) ≈ 6.9–5.8 kPa.

In stage 5, the fuel reactor temperature rose back to 900 °C. At the end of this period, the elutriated particles in the filter, which were 1280 g, were discharged and then fed into the fuel reactor.

In stage 6, after feeding the elutriated particles into the fuel reactor, the fuel reactor temperature decreased from 900 to 600 °C. The effect of fuel reactor temperature on gas conversion was studied again with more solid inventory in the system. Right after feeding the elutriated particles, the pressure drop of the fuel reactor increased to ~7 kPa, which was the same as the pressure after feeding all the fresh K10-ilmenite at the end of stage 2 in Figure 7. However, afterward, there was a gradual decrease of the fuel reactor pressure drop because of the particle elutriation. Within 4.4 h in stage 6, the fuel reactor pressure dropped from 7 to 6 kPa, with 513 g particles being elutriated again. Figure 9b reveals a magnification of the CO and $CO_2$ concentrations when the fuel reactor temperature decreased from 900 to 600 °C in stage 6 of Figure 7.

Both parts a and b of Figure 9 show that as the fuel reactor temperature decreased, the outlet CO concentration increased, with the $CO_2$ concentration decreasing, suggesting a lower CO conversion. This trend was the same as in the case of the pure raw ilmenite, as shown in Figure 5. However, at all the tested fuel reactor temperatures, with the presence of K10-ilmenite, the unconverted CO was much less. The CO concentration increased from 2.13% to 4.66% within 900–650 °C (Figure 9a) when the fuel reactor had a pressure drop of 4.3 kPa. When the fuel reactor pressure drop rose to 6.9–5.8 kPa by replacing the elutriated particles, the CO concentration was even less, only increasing from 1% to 2.63% (Figure 9b) within 900–650 °C. These unconverted CO concentrations were much less than that of the pure raw ilmenite, which increased from 3.77% to 7.40% in the same temperature range. The increase rate of the CO concentration along with the decrease of fuel reactor temperature was also different. The CO concentration increased more slowly with the existence of K10-ilmenite than in the case of pure raw ilmenite.

A detailed comparison of the CO conversion behavior with different bed materials at different fuel reactor temperatures was plotted in Figure 10. Again, the decrease of CO conversion with

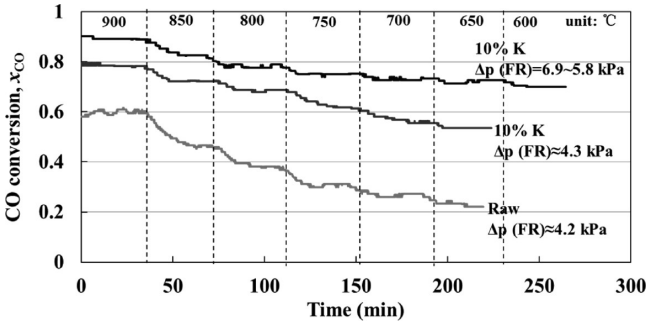


**Figure 10.** Conversion of CO at different fuel reactor temperatures for the raw ilmenite (raw—from stage 5 of Figure 3, $\Delta p$(FR) ≈ 4.2 kPa) and K10-ilmenite mixed with raw ilmenite (10% K—from stage 4 ($\Delta p$(FR) ≈ 4.3 kPa) and stage 6 ($\Delta p$(FR) = 6.9–5.8 kPa) of Figure 7).

temperature decreasing can be obviously seen. Even so, during the entire range of 900–650 °C, the bed material containing K10-ilmenite showed a much higher conversion of CO (78–54% when $\Delta p$(FR) ≈ 4.3 kPa; 89%~71% when $\Delta p$(FR) = 6.9–5.8 kPa) than the pure raw ilmenite (60–22% when $\Delta p$(FR) ≈ 4.2 kPa), especially at lower temperatures. Because of the promoted reactivity of K10-ilmenite, the gas conversion was even improved at lower temperatures, not just at 900 °C. Meanwhile, compared to the raw ilmenite, it can be noticed that the decrease of CO conversion was slower in the presence of K10-ilmenite. When the temperature dropped from 900–650 °C, the decrease of CO conversion was 24% ($\Delta p$(FR) ≈ 4.3 kPa) and 18% ($\Delta p$(FR) = 6.9–5.8 kPa) in the presence of K10-ilmenite, but it was up to 38% for the raw ilmenite with $\Delta p$(FR) ≈ 4.2 kPa. The case of K10-ilmenite with $\Delta p$(FR) = 6.9–5.8 kPa showed the smallest decrease of CO conversion; the CO conversion almost remained constant within 700–600


dx.doi.org/10.1021/ie4025209 | Ind. Eng. Chem. Res. 2013, 52, 14817–14827

°C, which was as high as 70% even at 600 °C. All of these indicated that the reduction reactivity of the used K10-ilmenite was not affected by temperatures as much as the raw ilmenite. Compared to stage 1 in Figure 7 (also shown in Figure 8), within 900−700 °C, the effect of temperature on the reactivity of the used K10-ilmenite was relatively larger than that for the fresh K10-ilmenite, but it was much less than that for the raw ilmenite. Overall, K10-ilmenite, no matter if it was the fresh or the used one, showed a high reduction reactivity in the wide temperature range 600−900 °C.

The presence of 10% $K^+$ not only promoted the ilmenite's reactivity but also weakened the effect of temperature on the reactivity. The limited effect of temperature on the reduction reactivity of K10-ilmenite is meaningful. It suggests that the fuel reactor of a CLC plant with K10-ilmenite as an oxygen carrier can be operated in a wide temperature window with a high performance being maintained. Stated in another way, the standards for the temperature of the fuel reactor can be lowered and there will be less impact on the performance of the CLC system even when the fuel reactor temperature fluctuates. In addition, the fuel reactor can be operated at a relatively low temperature, which demands less energy input. Although in CLC with solid fuels, such as coal, bringing the temperature down will decrease the gasification rate of coal,[18] there is the possibility that $K^+$ from K10-ilmenite particles provides a catalytic effect on promoting the gasification rate.[19,20] The application of K10-ilmenite in a CLC system with solid fuels deserves to be studied in the future. It is also interesting to discover the principle of the limited effect of temperature on the reactivity of K10-ilmenite.

In Figure 7, the first 30 min of stage 6 and the beginning of stage 3 had the same fuel reactor temperature (900 °C) and the same fuel reactor pressure drop, i.e., the same solid inventory in the fuel reactor. Under the same experimental conditions, the CO conversion was 89% (CO concentration: 1%) in stage 6 and 100% in stage 3. The decrease of CO conversion in the later stage 6 was due to the reactivity deterioration, as mentioned when discussing stage 3. It can be seen from here that although there was reactivity deterioration for K10-ilmenite, this deterioration was not distinct. Even after a continuous operation for 28 h (stage 3−5), the CO conversion only decreased from 100% to 89% at 900 °C when the fuel reactor pressure drop was ∼6.9 kPa. The 10% $K^+$ promoted ilmenite was one promising oxygen carrier for CLC.

During the entire 40 h operation, no trace of corrosion caused by potassium was found. This should be because only a small amount of potassium was added in the reactor. When applying this 10% $K^+$ promoted ilmenite in a large scale system, a larger bed inventory would be required, which corresponds to more potassium in the system. In this case, the downstream corrosion may not be avoided. In order to avoid the corrosion, additives, such as kaolin,[21] $SiO_2$, MgO, and $Al_2O_3$,[22] can be used to capture the released gas phase potassium. Meanwhile, the potassium volatilization process can be accomplished separately before running the promoted ilmenite in the large scale system. This is because the potassium volatilization mostly occurs during the transition from $K_2CO_3$ to the K-rich phase, i.e., $K_{1.46}Ti_{7.2}Fe_{0.8}O_{16}$.[15]

**3.3. Fragmentation and Attrition of the Ilmenite Oxygen Carriers.** At the end of each operation, the ilmenite particles from the reactor, the filter, and the fine particle collector were collected and analyzed. In both operations, there was negligible amount of particles in the filter connected to the fuel reactor due to a relatively low gas flow rate of the fuel reactor. Therefore, the following filters all denote the filter connected to the air reactor. Figure 11 shows the particle size distribution for the raw ilmenite and K10-ilmenite mixed with the used raw ilmenite from the reactor and the filter at the end of each operation, as measured by a laser particle size analyzer (Mastersizer 2000). The particle sizes of both bed materials in the reactor are nearly in the same range of the initial raw ilmenite. However, the particles elutriated from the cyclone to the filter have smaller sizes than those remaining in the reactor. 90 vol % of the particles in the filter are in the size range 85−235 $\mu$m, whereas 90 vol % of the particles in the reactor are in the size range 125−375 $\mu$m. The elutriation of the relatively small ilmenite particles from the reactor along with the fine particles caused by fragmentation and attrition are the reasons that the particles in the filter show a smaller size. This statement can be proven by the observation under a scanning electron microscope (SEM, JSM-7001F). Figure 12 shows the SEM images of the particles in the reactor, the filter, and the fine particle collector after 40 h of operation of K10-ilmenite mixed with the used raw ilmenite. The SEM images of the raw ilmenite particles after 100 h of operation, not given here, show similar characteristics. Figure 12b clearly shows that the particles in the filter contain particles elutriated from the reactor due to the low efficient cyclone, which are relatively smaller than the particles remaining in the reactor (Figure 12a). There are also fine particles appearing in the filter (Figure 12b), but not the reactor. The formation of the fine particles should be attributed to the fragmentation and attrition during fluidization and solid circulation. As seen from Figure 12c, fine particles (which have a size of only 3−4 $\mu$m) derived from fragmentation and attrition are also found in the end collector. Since the amount of the fine particles was too limited for the laser particle size analyzer, we cannot provide its size distribution as in Figure 11.

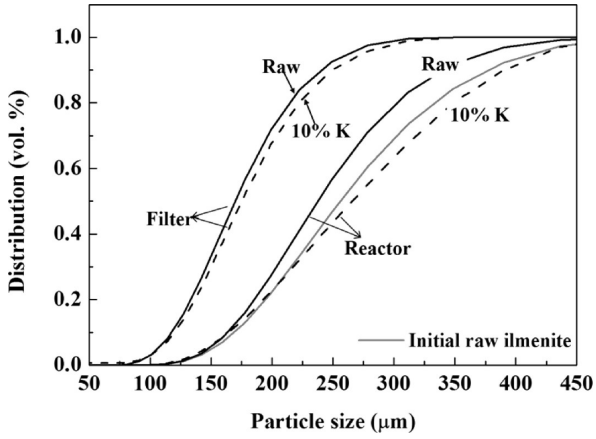


**Figure 11.** Particle size distribution for the raw ilmenite (Raw) and K10-ilmenite mixed with the used raw ilmenite (10% K) from the reactor and the filter at the end of each operation. The initial raw ilmenite is also included for comparison.

In order to find out the fragmentation and attrition ratio $\delta_m$, as defined by eq 3, the mass of the fine particles caused by fragmentation and attrition was taken. Table 2 lists the mass distribution in the system for the raw ilmenite and K10-ilmenite mixed with the used raw ilmenite at the end of 100 and 40 h operation, respectively. The calculation of $\delta_m$ is given as well. The fine particles in the filter were separated by sieving. Since


dx.doi.org/10.1021/ie4025209 | Ind. Eng. Chem. Res. 2013, 52, 14817−14827

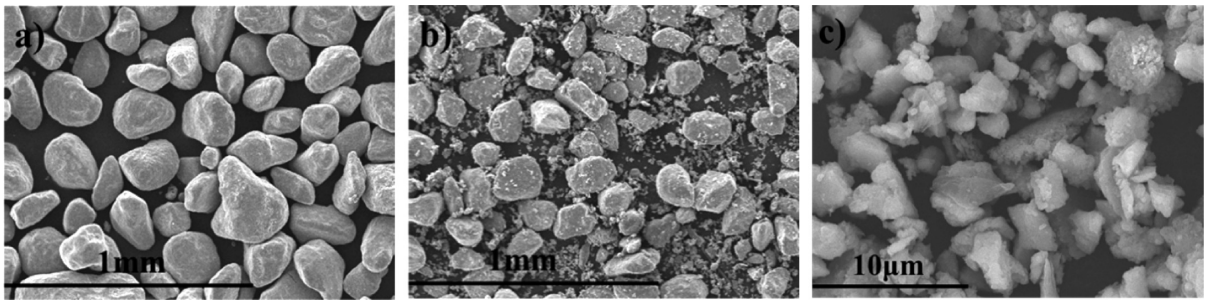


**Figure 12.** SEM images of the particles in (a) the reactor; (b) the filter; (c) and the fine particle collector after 40 h of operation of K10-ilmenite mixed with the used raw ilmenite. The particles after 100 h of operation of the raw ilmenite show similar characteristics.

**Table 2. Mass Distribution in the System for the Raw Ilmenite and K10-ilmenite Mixed with the Used Raw Ilmenite at the End of the 100 and 40 h Operations, Respectively**[a]

| | | filter (g) | | | | |
|---|---|---|---|---|---|---|
| | reactor (g) | <125 μm | 125−150 μm | collector (g) | total (g) | $\delta_m$ (%) |
| raw ilmenite | 5458.6 | 57.6 | 1779.9 | 5.9 | 7302.0 | 0.87 |
| K10-ilmenite | 6486.1 | 48.3 | 464.3 | 1.3 | 7000.0 | 0.71 |

[a]The fragmentation and attrition ratios $\delta_m$ are calculated.

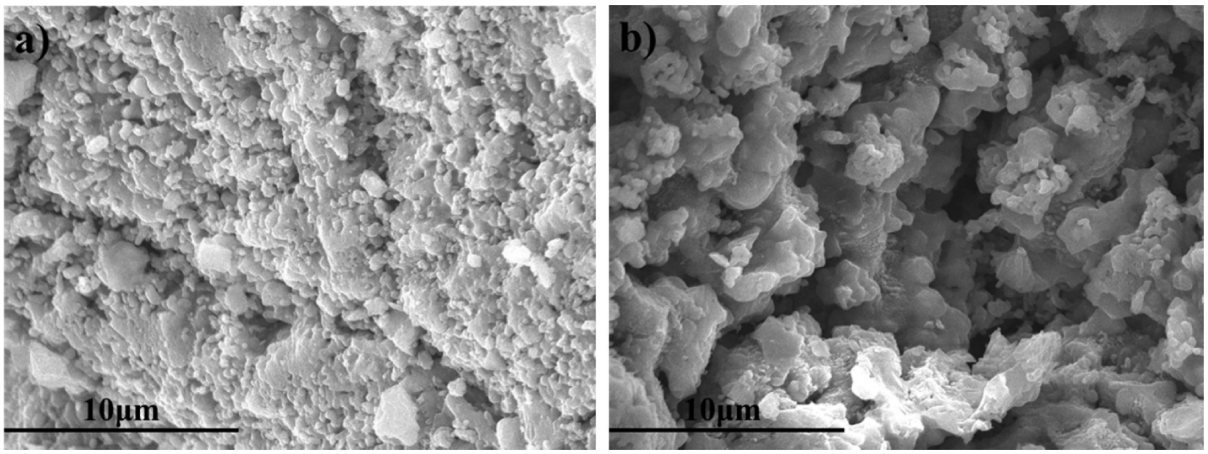


**Figure 13.** Internal SEM images of the (a) raw ilmenite and the (b) K10-ilmenite mixed with the used raw ilmenite in the reactor after 100 and 40 h operation, respectively.

the initial raw ilmenite particle was in the range 125−300 μm, the particles smaller than 125 μm were produced by fragmentation and attrition, and the ones in the range 125−150 μm were elutriated because of the inefficient cyclone. The size here by sieving is a little different from the one shown in Figure 11. This difference may be because of the analysis method or the deviation of the laser particle size analyzer. The total amount of the fine particles in the filter (<125 μm) and the collector was the mass loss caused by fragmentation and attrition. By dividing this mass loss by the total solid inventory in the system, the fragmentation and attrition ratio $\delta_m$ can be known. The calculated $\delta_m$ is 0.87% for the raw ilmenite after 100 h and 0.71% for K10-ilmenite mixed with the used raw ilmenite after 40 h. This result clearly shows that the fragmentation and attrition of the ilmenite particles, no matter the raw or the K promoted one, is not obvious during long-term operation. Both ilmenite oxygen carriers show good mechanical strength and stability.

**3.4. Characterization of the Ilmenite Carriers.** The particles of the raw ilmenite and K10-ilmenite mixed with the used raw ilmenite in the reactor at the end of each continuous operation were observed under a SEM. Figure 13 shows the internal structures of both types of particles. Considering the heterogeneous structure of the natural ilmenite ore, during the SEM test, all particles in each batch were observed; most of them showed a similar morphological character. In Figure 13, both ilmenite carriers show porous structures. However, the particles with the presence of K10-ilmenite are much more porous, as shown in Figure 13b. The porous structure of the raw ilmenite is obtained by the activation process.[7−9,15] With the existence of K10-ilmenite, the migration or diffusion of $K^+$ further develops the pore structure and increases the porosity. The pore promoting effect of $K^+$ and quantification of the porosity increase have been studied in detail in the previous work.[15] It should be emphasized that the more porous structure in Figure 13b is found on the mixture of K10-ilmenite and the used raw ilmenite, which is not only on the K10-ilmenite particle itself but also on the raw ilmenite particle. This means that the attendance of $K^+$ helps promote not only the pore structure of K10-ilmenite but also the surrounding raw ilmenite. This phenomenon suggests that the released $K^+$ from volatilization could deposit on the surface of the raw ilmenite


dx.doi.org/10.1021/ie4025209 | Ind. Eng. Chem. Res. 2013, 52, 14817−14827

particle, migrate inside the particle during chemical reactions, and finally promote the pore structure of the raw ilmenite. A detailed study of the fate of potassium and the related mechanisms for potassium degradation should be carried out in the future.

## 4. CONCLUSIONS

100 h continuous tests of raw ilmenite oxygen carriers and 40 h continuous tests of the 10% $K^+$ promoted ilmenite mixed with the used raw ilmenite were conducted in a dual interconnected fluidized bed reactor system. Successful and long-term operations with CO as reducing gas were accomplished under stable and well controlled conditions. The long-term operation results showed that raw ilmenite had a low reduction reactivity. At 900 °C, there was a complete CO conversion within the first 13.7 h when the fuel reactor pressure drop was 6.2 kPa; however, afterward, the CO conversion dropped to only ∼60% when the fuel reactor pressure drop was 4.2 kPa. By impregnating 21% of the total used raw ilmenite with 10% $K^+$, the CO conversion was improved to over 78.5% at 900 °C, with a similar fuel reactor pressure drop of 4.3 kPa attributed to an enhanced reduction reactivity of the $K^+$ modified ilmenite. Although there was reactivity deterioration of 10% $K^+$ promoted ilmenite due to the volatilization of $K^+$, this deterioration was not distinct. Even after 28 h of continuous operation, the CO conversion only decreased from 100% to 89% at 900 °C with the fuel reactor pressure drop of ∼6.9 kPa.

The effect of different operation parameters on gas conversion with raw ilmenite was studied. Either increasing the gas flow rate or decreasing the temperature of the fuel reactor resulted in a reduced CO conversion. The increase of the solid circulation rate by raising the secondary air could improve the CO conversion slightly. The critical parameters for gas conversion were the fuel reactor parameters, especially the fuel reactor temperature, which affected ilmenite's reactivity. The reduction reactivity of the 10% $K^+$ promoted ilmenite was not affected by temperatures as much as the raw ilmenite. With the existence of this promoted ilmenite, the CO conversion only decreased by ∼18% from 900 to 600 °C when the fuel reactor pressure was 6.9−5.8 kPa. This promoted ilmenite can be operated in a wide temperature range.

During both extended operations, no sintering or agglomeration was found. The mass losses caused by fragmentation and attrition were also low, which were only 0.87% and 0.71% of the total solid inventory after the 100 and 40 h operation, respectively. Both ilmenite carriers showed suitable mechanical strength and stability.

## AUTHOR INFORMATION

### Corresponding Author

*Telephone: 86-10-62781741. Fax: 86-10-62770209. E-mail: lizs@mail.tsinghua.edu.cn.

### Notes

The authors declare no competing financial interest.

## ACKNOWLEDGMENTS

This work was supported by the National Natural Science Foundation of China (51376105, 51061130535), the National Key Basic Research and Development Program (2011CB707301), the International S&T Cooperation Project of China (2013DFB60140), the Tsinghua University Initiative Scientific Research Program, and the Program for New Century Excellent Talents in University (NCET-12-0304).

## REFERENCES

(1) Richter, H.; Knoche, K. Reversibility of combustion processes. *ACS Symp. Ser.* **1983**, *235*, 71.

(2) Ishida, M.; Jin, H. $CO_2$ recovery in a power plant with chemical looping combustion. *Energy Convers. Manage* **1997**, *38*, S187.

(3) Shulman, A.; Linderholm, C.; Mattisson, T.; Lyngfelt, A. High reactivity and mechanical durability of $NiO/NiAl_2O_4$ and $NiO/NiAl_2O_4/MgAl_2O_4$ oxygen carrier particles used for more than 1000 h in a 10 kW CLC reactor. *Ind. Eng. Chem. Res.* **2009**, *48*, 7400.

(4) Kolbitsch, P.; Bolhar-Nordenkampf, J.; Proll, T.; Hofbauer, H. Comparison of two Ni-based oxygen carriers for chemical looping combustion of natural gas in 140 kW continuous looping operation. *Ind. Eng. Chem. Res.* **2009**, *48*, 5542.

(5) de Diego, L. F.; García-Labiano, F.; Gayán, P.; Celaya, J.; Palacios, J. M.; Adanez, J. Operation of a 10 kWth chemical-looping combustor during 200 h with a CuO-Al2O3 oxygen carrier. *Fuel* **2007**, *86*, 1036.

(6) Lyngfelt, A. Oxygen carriers for chemical-looping combustion—4000 h of operational experience. *Oil Gas Sci. Technol.—Rev. IFP Energies nouvelles* 2001, *66*, 161, DOI: 10.2516/ogst/2010038.

(7) Adanez, J.; Cuadrat, A.; Abad, A.; Gayán, P.; de Diego, L. F.; García-Labiano, F. Ilmenite activation during consecutive redox cycles in chemical-looping combustion. *Energy Fuels* **2010**, *24*, 1402.

(8) Abad, A.; Adanez, J.; Cuadrat, A.; García-Labiano, F.; Gayán, P.; de Diego, L. F. Kinetics of redox reactions of ilmenite for chemical-looping combustion. *Chem. Eng. Sci.* **2011**, *66*, 689.

(9) Leion, H.; Lyngfelt, A.; Johansson, M.; Jerndal, E.; Mattisson, T. The use of ilmenite as an oxygen carrier in chemical-looping combustion. *Chem. Eng. Res. Des.* **2008**, *86*, 1017.

(10) Azis, M. M.; Jerndal, E.; Leion, H.; Mattisson, T.; Lyngfelt, A. On the evaluation of synthetic and natural ilmenite using syngas as fuel in chemical-looping combustion (CLC). *Chem. Eng. Res. Des.* **2010**, *88*, 1505.

(11) Cuadrat, A.; Abad, A.; García-Labiano, F.; Gayán, P.; de Diego, L. F.; Adánez, J. The use of ilmenite as oxygen-carrier in a 500 Wth chemical-looping coal combustion unit. *Int. J. Greenhouse Gas Control* **2011**, *5*, 1630.

(12) Berguerand, N.; Lyngfelt, A. Batch testing of solid fuels with ilmenite in a 10 kWth chemical-looping combustor. *Fuel* **2010**, *89*, 1749.

(13) Bidwe, A. R.; Mayer, F.; Hawthorne, C.; Charitos, A.; Schuster, A.; Scheffknecht, G. Use of ilmenite as an oxygen carrier in chemical looping combustion—batch and continuous dual fluidized bed investigation. *Energy Procedia* **2011**, *4*, 433.

(14) Markström, P.; Lyngfelt, A.; Linderholm, C. Chemical looping combustion in a 100 kW unit for solid fuels. In *21st International Conference on Fluidized Bed Combustion*, June 3−6, Naples, Italy, 2012.

(15) Bao, J.; Li, Z.; Cai, N. Promoting the reduction reactivity of ilmenite by introducing foreign ions in chemical looping combustion. *Ind. Eng. Chem. Res.* **2013**, *52*, 6119.

(16) Bao, J.; Li, Z.; Cai, N. Reduction kinetics of foreign ion promoted ilmenite using carbon monoxide (CO) for chemical looping combustion. *Ind. Eng. Chem. Res.* **2013**, *52*, 10646.

(17) Lyngfelt, A.; Leckner, B.; Mattisson, T. A fluidized-bed combustion process with inherent CO2 separation; application of chemical-looping combustion. *Chem. Eng. Sci.* **2001**, *56*, 3101.

(18) Leion, H.; Mattisson, T.; Lyngfelt, A. Solid fuels in chemical-looping combustion. *Int. J. Greenhouse Gas Control* **2008**, *2*, 180.

(19) Yang, J.; Cai, N.; Li, Z. Hydrogen production from the steam-iron process with direct reduction of iron oxide by chemical looping combustion of coal char. *Energy Fuels* **2008**, *22*, 2570.

(20) Gu, H.; Shen, L.; Xiao, J.; Zhang, S.; Song, T.; Chen, D. Iron ore as oxygen carrier improved with potassium for chemical looping combustion of anthracite coal. *Combust. Flame* **2012**, *159*, 2480.

(21) Tran, K. Q.; Iisa, K.; Hagström, M.; Steenari, B. M.; Lindqvist, O.; Pettersson, J. B. C. On the application of surface ionization

detector for the study of alkali capture by kaolin in a fixed bed reactor. *Fuel* **2004**, *83*, 807.
(22) Sun, D.; Sung, W.; Chen, R. The release behavior of potassium and sodium in the biomass high-temperature entrained-flow gasification. *Appl. Mech. Mater.* **2011**, *71*−*78*, 2434.